

Bifunctional aminosilane-functionalized Fe₃O₄ nanoparticles as efficient sorbent for preconcentration of cobalt ions from food and water samples

Zahra Shaleri Kardar¹ · Mostafa Hossein Beyki¹ · Farzaneh Shemirani¹

Received: 30 November 2016 / Accepted: 4 January 2017 / Published online: 23 January 2017
© Springer Science+Business Media Dordrecht 2017

Abstract Magnetic Fe₃O₄ nanoparticles were synthesized by a coprecipitation method, then their surface was covered and modified by [1-(2-aminoethyl)-3-aminopropyl]trimethoxysilane. The resulting adsorbent was used in preconcentration of Co(II) ions prior to their determination by flame atomic absorption spectroscopy. The modified nanoparticles were characterized by Fourier-transform infrared spectroscopy, scanning electron microscopy, and vibrating-sample magnetometry techniques. Various parameters influencing the preconcentration efficiency, such as medium pH, adsorbent quantity, sample volume, and elution conditions, were optimized. Under optimum conditions, the analytical performance of the method was evaluated. The calibration curve was found to be linear from 1 to 200 µg L⁻¹ ($R^2 = 0.99$). The limit of detection was calculated to be 0.5 µg L⁻¹ ($n = 5$). The relative standard deviation was obtained as 2.5% ($n = 5$). Moreover, the maximum adsorption capacity of the sorbent was 32.05 mg g⁻¹. Kinetic and isotherm models were also studied, showing that the adsorption matched well with pseudo-second-order and Langmuir models. The ability of the developed method was proved by application for preconcentration of cobalt ions from food and water samples.

Keywords Cobalt · Food · Magnetic solid-phase extraction · Nanoparticles

✉ Mostafa Hossein Beyki
mhosseinbaki@yahoo.com

¹ School of Chemistry, University College of Science, University of Tehran, P.O. Box 14155-6455, Tehran, Iran

Introduction

Cobalt, as a naturally occurring element, is considered to be an essential trace metal. Among its two oxidation states, i.e., Co(II) and Co(III), the former is more stable. It has only one stable isotope (^{59}Co), as well as 28 radioisotopes, the most stable of which is ^{60}Co with half-life of 5 years, producing two high-energy γ photons [1]. One important source for release of radioactive cobalt to the environment may be inappropriate dumping of radioactive waste from nuclear power plants or medical centers using radioactive cobalt for radiotherapy or equipment sterilization [2]. The nonradioactive isotope of cobalt may be released into the environment by natural phenomena such as volcanic eruptions and forest fires, or through its application in industrial, agricultural, medical, and artistic activities [3]. This form of cobalt is an essential element for humans, as it plays an important role in blood formation processes [4, 5]. However, it can have adverse effects on the human body, including asthma, pneumonia, wheezing, skin rashes, and vomiting [6], when entering the body above the limit of 0.005–0.010 mg day⁻¹ [7]. Considering both the beneficial and hazardous impacts of cobalt on humans and other living organisms, reliable and sensitive analytical methods for its determination in water, food, environmental, and clinical samples are required [8, 9].

Flame atomic absorption spectroscopy (FAAS) is one of the most regularly used methods for determination of metal ions. However, this valuable method suffers from two main limitations: an inappropriate detection limit for some metals, and the presence of an interfering matrix which can affect the selectivity and sensitivity of the method [10–12]. To overcome these restrictions, preconcentration techniques can be applied to concentrate the analyte ions in a new, noninterfering matrix [13–15]. There are many different methods to achieve this, ranging from the classic conventional liquid–liquid extraction approach to more contemporary techniques based on microextraction [16, 17]; however, in recent decades, solid-phase extraction has become the most widely employed and favored approach [18, 19], owing to its economical, rapid, green, and robust characteristics as well as its ability to achieve high enrichment factors and recoveries [20–22].

Magnetic solid-phase extraction (MSPE), as a new mode of SPE, has aroused strong interest and attention from researchers since its introduction in 1999 [23–25]. In this method, magnetic or magnetically modified particles as adsorbents can be easily and quantitatively separated from the extraction medium by applying an external magnetic field [26, 27].

There are a number of types of magnetic particles with ferromagnetic or superparamagnetic properties, differing in size from nano- to micrometers [28, 29]. Among these, the most popular are Fe_3O_4 nanoparticles (NPs), as they combine magnetic properties with the features of nanoparticles, possessing characteristics such as high surface-to-volume ratio, easy separation from sample solution, good reusability, good biocompatibility, and nontoxicity [30, 31]. Fe_3O_4 NPs can be prepared by various methods, but the conventional approach is coprecipitation [32]. Bare Fe_3O_4 NPs tend to aggregate and are prone to oxidation in air or dissolution in acidic conditions. Moreover, they lack selectivity toward target analytes in complex

matrices [33]. One way to overcome these obstacles is to functionalize the surface of NPs using an appropriate ligand [34].

Organosilicates are bifunctional compounds that have been widely used for surface modification of different materials, especially magnetic nanoparticles (MNPs). [1-(2-Aminoethyl)-3-aminopropyl]trimethoxysilane (AEAPTMS) is a member of this category that can be hydrolyzed to produce silanol groups on the surface of NPs as a polymeric coating. Meanwhile, the terminal functional group (–NH–CH₂–CH₂–NH₂) at the other end of this molecule can act as a chelating agent for cobalt ions. Therefore, this coating not only stabilizes Fe₃O₄ NPs but also increases their extraction capability toward target ions [35–37].

In this study, AEAPTMS-modified Fe₃O₄ NPs were synthesized by a fast, simple method and used for preconcentration of cobalt ions. It was found that these NPs can act as a stable and efficient superparamagnetic adsorbent for preconcentration of cobalt ions prior to their determination by FAAS. In addition, the adsorption behavior and analytical performance of the proposed method were studied in detail. Finally, the suitability and applicability of the method were evaluated by applying it for preconcentration of cobalt ions from different water and food samples.

Experimental

Materials

All applied chemicals were of analytical reagent grade. All metal salts and stock solution of cobalt (1000 mg L⁻¹) were prepared by dissolving appropriate amounts of Co(NO₃)₂ salt into HNO₃ (1.0 mol L⁻¹) solution, diluted to the mark on a 100-mL volumetric flask. Calibration and test solutions were prepared daily by suitable dilution of stock solution with distilled water. All stock standard solutions were stored in polyethylene bottles in ambient condition. Co(NO₃)₂·6H₂O, Fe(NO₃)₃·9H₂O, FeSO₄·7H₂O, and glacial acetic acid were purchased from Merck (Darmstadt, Germany). Methanol [high-performance liquid chromatography (HPLC) grade] and AEAPTMS (80%) were supplied by Sigma Aldrich Co. Solution pH was adjusted to the desired value by adding HCl and NH₃ (0.5 mol L⁻¹) solution.

Instruments

A Varian model AA-400 atomic absorption spectrometer with deuterium background corrector was used for determination of analyte ions in samples. All measurements were carried out in an air/acetylene flame with a cobalt hollow cathode lamp as radiation source. The instrumental operating conditions for the element were set as recommended by the manufacturer. A Metrohm model 692 pH meter equipped with a glass combination electrode was used for pH adjustment. Fourier-transform infrared (FTIR) spectra were obtained using an Equinox 55 (Bruker Optik GmbH, Ettlingen, Germany) in attenuated total reflection (ATR) mode in the wavelength range from 400 to 4000 cm⁻¹. Field-emission scanning

electron microscopy (FE-SEM) was carried out using Hitachi S-4160 instruments. Magnetization measurements were performed using a vibration-sample magnetometer (VSM; model 7400, Lake Shore Cryotronics, Inc., Westerville, OH).

Adsorbent synthesis

Synthesis of magnetic nanoparticles

Fe_3O_4 magnetic nanoparticles were prepared by an ultrasound-assisted precipitation route. Briefly, 8.7 g $\text{Fe}(\text{NO}_3)_3 \cdot 9\text{H}_2\text{O}$ and 2.9 g $\text{FeSO}_4 \cdot 7\text{H}_2\text{O}$ were dissolved in 200 mL deionized water, then sonicated until clear solution was obtained. Afterward, the temperature of the sonication bath was adjusted to 80 °C. At this temperature, 5 mL concentrated ammonia solution was added to the mixture immediately, and ultrasonic agitation was continued for 30 min. Then, it was allowed to cool down to room temperature, and the obtained Fe_3O_4 nanoparticles were separated from the mixture by a magnet then repeatedly washed with deionized water followed by drying at 80 °C for 2 h.

Functionalization of magnetic nanoparticles

For this purpose we applied a silanation protocol as reported by Dupont et al. [38] with small changes. Freshly synthesized Fe_3O_4 nanoparticles (2.5 g) were added to a beaker containing 100 mL methanol, which was then placed in an ultrasonic bath for 1 h to achieve good dispersion. Then, 5 mL AEAPTMS was added together with a few drops of glacial acetic acid, followed by sonication at 50 °C for 3 h. The modified nanoparticles were separated from the reaction mixture using a magnet and washed three times with acetone and two times with water, finally being dried at room temperature for 1 day. The preparation process is illustrated schematically in Fig. 1.

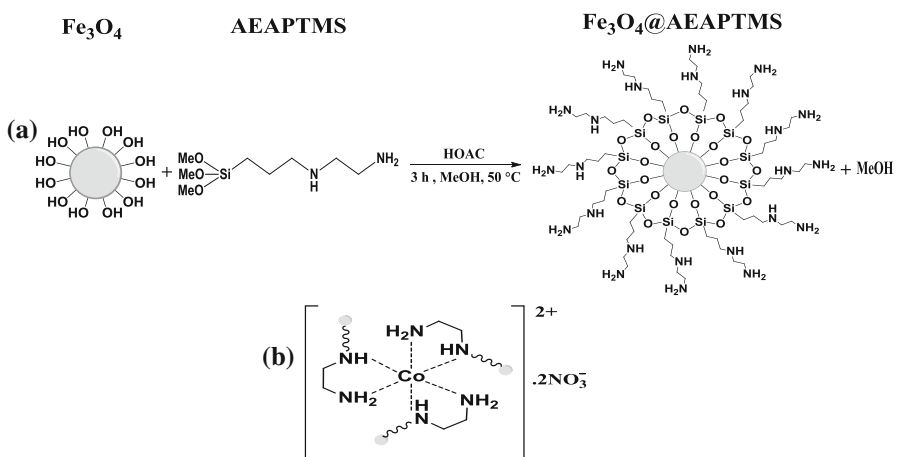


Fig. 1 **a** Schematic of synthesis of $\text{Fe}_3\text{O}_4@$ AEAPTMS. **b** Illustration of cobalt ions complexed with AEAPTMS on the adsorbent surface

Preconcentration procedure

Batch experiments were conducted to investigate the adsorption of Co(II) ions from sample solutions by the adsorbent. Adsorbent (0.05 g) was added into a 50 mL tube containing 5 µg Co(II) ions at pH 8.0, followed by sonication for 1 min to achieve good dispersion. To achieve the adsorption process, it was shaken for 20 min. Then, the adsorbent was aggregated by placing the container on a magnet, and the supernatant was completely decanted. In the desorption step, the analyte retained on the adsorbent was diluted by adding 5 mL 1 mol L⁻¹ HNO₃ solution to the separated solid and shaking for 10 min. Finally, eluted ions were determined by FAAS.

Real sample pretreatment

Preparation of water samples

A tap water sample was obtained from our laboratory (University of Tehran). A sea water sample was collected from the Caspian Sea, and kept in a bottle in acidic medium. To remove suspended particles, the sea water sample was filtered through filter paper before use. After pH adjustment, 50 mL of each sample was submitted to the proposed method.

Preparation of food samples

All food samples were purchased from a local market in Tehran. Amounts of 2.0 g instant coffee powder, shrimp, soya, radish, and wheat bud powder and 50 mL malt beverage were dried separately in an oven for about 1 h. When a steady weight of each sample was obtained, it was cooled down and submitted to a digestion process in which 10 mL HNO₃ solution (65%) was added to each sample, followed by gentle heating until evolution of brown fumes ceased. Then, 10 mL 30% hydrogen peroxide was added to each solution, and slight heating was continued until complete decomposition of each sample resulted in clear solution. The residues were cooled down to room temperature, diluted with water, and filtered through filter paper. The solution pH was adjusted to 8, and the volume made up to 200 mL with distilled water in a volumetric flask. Finally, the proposed method was applied to 50 mL of each sample.

Results and discussion

Characterization of adsorbent

The FTIR spectrum is shown in Fig. 2a. Presence of magnetite nanoparticles is indicated by two strong absorption bands at around 517 and 564 cm⁻¹, resulting from splitting of the ν_1 band at 570 cm⁻¹, which corresponds to Fe–O bond of bulk magnetite. Furthermore, an adsorption band was observed at around 457 cm⁻¹, corresponding to the shifted ν_2 band of Fe–O bond at 375 cm⁻¹ to higher

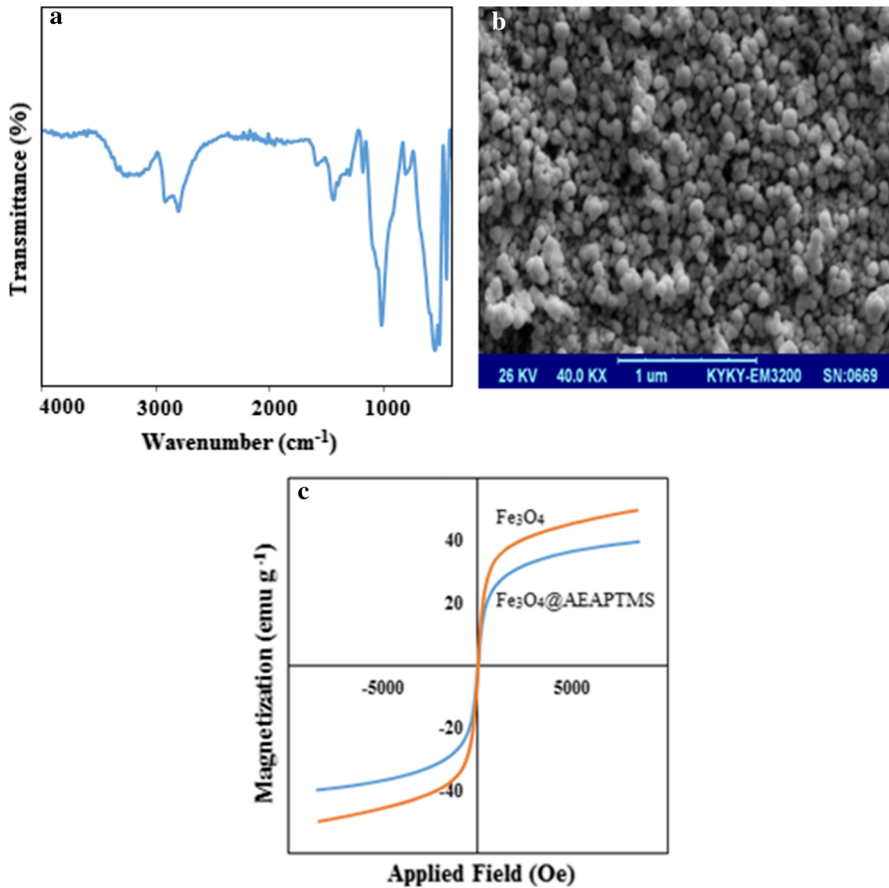


Fig. 2 a FTIR spectrum of Fe₃O₄@AEAPTMS, b SEM micrograph of Fe₃O₄@AEAPTMS, c VSM curves of bare Fe₃O₄ and Fe₃O₄@AEAPTMS

wavenumber. The silica network was adsorbed on the magnetite surface by Fe–O–Si bonds. This adsorption band cannot be seen in the FTIR spectrum because it appears at around 584 cm⁻¹ and therefore overlaps with the signal for Fe–O vibration of the magnetite nanoparticles. However, the adsorption of silane polymer onto the surface of the magnetite particles was confirmed by the band at 1028 and shoulder at 934 cm⁻¹, assigned to SiO–H and Si–O–Si groups. The absorption band at 817 cm⁻¹ reveals the presence of OH vibration on the surface of magnetite. The two broad bands at 3256 and 1601 cm⁻¹ can be ascribed to the N–H stretching vibration and NH₂ bending mode of free NH₂ group, respectively. Furthermore, hydrogen-bonded silanol also absorbs at around 3200 and 470 cm⁻¹. Presence of anchored propyl group was confirmed by the C–H stretching vibration signal at 2929 cm⁻¹.

To study the surface morphology of the adsorbent, the samples were characterized by FE-SEM. The image of the solid in Fig. 2b shows spherical morphology and uniform (homogeneous) dispersion of the particles. The average diameter of the

modified Fe₃O₄ nanoparticles as estimated from the micrograph was approximately 50 nm.

The magnetization curve of bare Fe₃O₄ and Fe₃O₄@AEAPTMS was measured at room temperature using a vibrating-sample magnetometer. As shown in Fig. 2c, the magnetic hysteresis loops showed an S-like curve with specific saturation magnetization (M_s) of 49.8 and 39.7 emu g⁻¹ for Fe₃O₄ and Fe₃O₄@AEAPTMS, respectively. The decrease in the magnetization value is due to the coating of AEAPTMS around the magnetic core. However, this value is still adequate for the solid to be used in the MSPE procedure.

Optimization of preconcentration procedure

Effect of pH

The pH of the medium plays a critical role in extraction of heavy metals onto adsorbents, not only affecting the surface charge of the adsorbent but also influencing the speciation of the metal ions in solution. The effect of this parameter on the extraction efficiency of Co(II) ions on the adsorbent was studied in the pH range of 3–9. The results (Fig. 3a) show that, while the absorption efficiency was near zero at pH 3, it rose with increasing pH, showing quantitative adsorption (>95%) at pH 8. This observation is consistent with the metal–amine complexation adsorption mechanism. At low pH, amine groups are protonated, hence these adsorption sites become passive and metal adsorption is suppressed. As the difference in the removal percentage of Co(II) at pH 8 and 9 was small, and partial precipitation of Co(OH)₂ is likely at pH 9 at higher concentrations, we chose pH 8 as the optimum value for further experiments.

Effect of eluent type, concentration, and volume

The effect of the eluent type on the release of adsorbed Co(II) ions from the modified adsorbent was examined by applying a series of solutions with concentration of 1.0 mol L⁻¹ (HNO₃, HCl, CH₃COOH), ethanol, and 1:1 mixture of ethanol:HNO₃ (1 mol L⁻¹). The results showed that HNO₃ solution gave much higher elution efficiency (>95%) compared with other eluents. Choosing HNO₃ as eluent, the effect of its volume on the quantitative elution of Co(II) ions was investigated over the range of 1–5 mL. Based on the results (Fig. 3b), the maximum elution efficiency was obtained when using 5 mL of eluent. Thus, this volume was chosen for further studies. In the next step, the effect of the HNO₃ concentration on the elution step was evaluated by testing different concentrations from 1 to 2.5 mol L⁻¹. However, it was found that changing this parameter had no obvious effect on the desorption efficiency; at any concentration of acid, the recovery percentage was near to 100%.

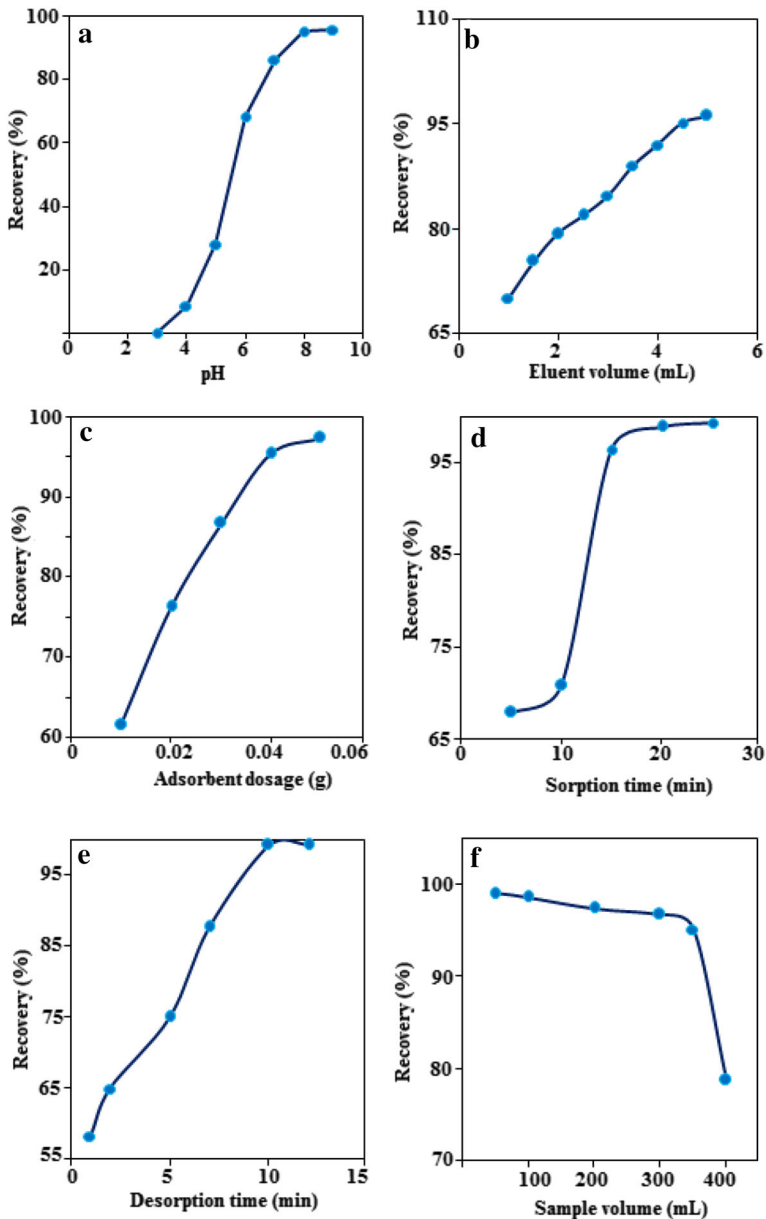


Fig. 3 Effects of **a** initial pH (conditions: pH 3–9, sorbent 0.05 g, concentration 0.05 mg L^{-1} , sample volume 50 mL, contact time 20 min), **b** elution volume (conditions: pH 8, sorbent 0.05 g, concentration 0.05 mg L^{-1} , sample volume 50 mL, elution volume 1–5 mL, contact time 20 min, desorption time 10 min), **c** amount of sorbent (conditions: pH 8, sorbent 0.01–0.05 g, concentration 0.05 mg L^{-1} , sample volume 50 mL, contact time 20 min), **d** contact time (conditions: pH 8, sorbent 0.05 g, concentration 0.05 mg L^{-1} , sample volume 50 mL, contact time 5–25 min), **e** desorption time (conditions: pH 8, sorbent 0.05 g, concentration 0.05 mg L^{-1} , sample volume 50 mL, elution volume 5 mL, contact time 20 min, desorption time 1–12 min), and **f** sample volume (conditions: pH 8, sorbent 0.05 g, concentration 0.05 mg L^{-1} , sample volume 50–400 mL, elution volume 5 mL, contact time 20 min, desorption time 10 min) on recovery of Co(II) ions

Effect of sorbent amount

Different quantities of adsorbent in the range of 0.01–0.05 g were tested to determine the least sorbent amount that still gave the maximum adsorption efficiency. The plot of recovery percentage versus sorbent amount in Fig. 3c shows that quantitative sorption occurred when 0.05 g adsorbent was used. So, a sorbent amount of 0.05 g was selected in following experiments.

Effect of contact time

We also investigated the effect of the shaking time on the recovery of Co(II) ions to determine an appropriate equilibrium time. The recovery was evaluated when using durations in the range of 5–25 and 1–12 min for the sorption and desorption process, respectively. The results are illustrated in Fig. 3d, e. As can be seen, the appropriate time to establish Co(II) ion adsorption equilibrium was 20 min, whereas it was 10 min for the desorption process, indicating that both processes showed good kinetics.

Effect of sample breakthrough volume

In analysis of real samples, the sample volume is one of the important parameters affecting the enrichment factor. To study the effect of the sample volume on the extraction of Co(II) ions, sample volumes of 50–400 mL containing fixed amounts of metal ion (100 µg) were used. Based on the results (Fig. 3f), it was found that quantitative recovery (>95%) was achieved for sample volumes up to 350 mL. For larger volumes, the analyte recoveries decreased slightly, hence 350 mL was selected as the breakthrough volume. After release of adsorbed ions using 5 mL eluent, an enrichment factor of 70 was obtained for Co(II) ions using the proposed method.

Effect of coexisting ions

Diverse ions present in the experimental environment or sample matrix may interfere with the determination of a target analyte ion. The effect of some of the most probable of these ions on the recovery of the Co(II) ions from the adsorbent was investigated by adding various amounts of them individually to 50 mL test solutions containing 0.05 mg L⁻¹ Co(II) ions, then applying the general preconcentration procedure described above. The results in Table 1 show that, even at high levels, potential interfering ions had no effect on the preconcentration of Co(II) ions by this method. Thus, the proposed method can be applied to determine the target analyte in complicated matrix samples.

Sorption kinetics

Almost any sorption/desorption process in solid-phase extraction studies is time dependent. To understand the dynamic interactions of the adsorbate with the sorbent

Table 1 Effect of interfering ions on preconcentration of Co(II) ions

Conditions: pH 8, sorbent 0.05 g, cobalt concentration 0.05 mg L⁻¹, sample volume 50 mL, elution volume 5 mL, contact time 20 min, desorption time 10 min

Ion	Tolerance limit (mg L ⁻¹)
Na ⁺ , K ⁺	100
Mg ²⁺ , Ca ²⁺	50
Pb ²⁺ , Cd ²⁺ , Zn ²⁺ , Cu ²⁺ , Ni ²⁺	5
NO ₃ ⁻ , Cl ⁻	100
PO ₄ ³⁻ , CO ₃ ²⁻	50

and predict their response as a function of time, knowledge about the kinetics of these processes is beneficial. For this purpose, various kinetic models have been used by researchers [39], whereas in this study the pseudo-first-order and pseudo-second-order models were adopted to analyze equilibrium data. Kinetic experiments were carried out by applying the same SPE protocol described above with different selected contact times ranging from 5 to 20 min. The results of fitting these data to the mentioned kinetic models are listed in Table 2, and the plots are depicted in Fig. 4.

The pseudo-first-order model is widely used for adsorption of an adsorbate from aqueous solution, being generally expressed as

$$\frac{dQ}{dt} = K_1(Q_e - Q_t), \quad (1)$$

where K_1 (g mg⁻¹ min⁻¹) is the pseudo-first-order rate constant, Q_e (mg g⁻¹) is the amount of solute sorbed at equilibrium, and Q_t (mg g⁻¹) is the amount of solute sorbed on the surface of the sorbent at any time t . When integrated with the boundary conditions $Q_t = 0$ at $t = 0$ and Q_t at time t , this equation becomes

$$\ln(Q_e - Q_t) = \ln Q_e - K_1 t. \quad (2)$$

The adsorption rate constant (K_1) was calculated from plots of $\ln(Q_e - Q_t)$ against t [40]. The pseudo-second-order model can be expressed as

$$\frac{dQ_t}{dt} = K_2(Q_e - Q_t)^2, \quad (3)$$

where K_2 is the pseudo-second-order rate constant (g mg⁻¹ min⁻¹). Integration of this equation with the boundary conditions $Q = 0$ at $t = 0$ and $Q = Q_t$ at $t = t$ results in

Table 2 Constants for pseudo-first-order and pseudo-second-order models for adsorption of Co(II) ions

Pseudo first order			Pseudo second order		
Q_e (mg g ⁻¹)	K_1 (min ⁻¹)	R^2	Q_e (mg g ⁻¹)	K_2 (g mg ⁻¹ min ⁻¹)	R^2
0.050	0.072	0.8466	0.120	1.55	0.9416

Conditions: pH 8, sorbent 0.05 g, concentration 5 mg L⁻¹, sample volume 50 mL, contact time 5–20 min

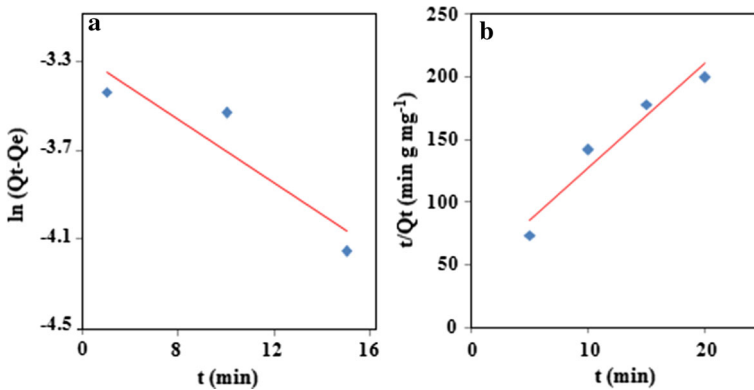


Fig. 4 **a** First-order and **b** second-order plots for Co(II) adsorption on AEAPTMS-coated Fe₃O₄ nanoparticles (conditions: pH 8, dosage 0.05 g, sample volume 50 mL)

$$\frac{t}{Q_t} = \frac{1}{K_2 Q_e^2} + \left(\frac{1}{Q_e}\right)t. \quad (4)$$

The Q_e and K_2 values can be obtained from linear plots of $\frac{t}{Q_t}$ versus t [41–43]. Based on the linear regression correlation coefficient (R^2) values, the data were well fit by the pseudo-second-order kinetic model. Moreover, the Q_e value obtained based on the second-order model was close to the experimental value and showed lower deviation relative to the first-order model, further confirming that the adsorption mechanism was second order.

Sorption isotherm

Adsorption isotherms are mathematical models that describe the distribution of an adsorbate species between liquid and solid phases at constant temperature. These models are based on a set of assumptions related to the heterogeneity or homogeneity of the solid surface, the type of coverage, and the possibility of interaction between the adsorbate species. There are a number of applicable isotherms [44], however, in this study, equilibrium data for cobalt ions were analyzed using three of the most famous ones: Freundlich, Langmuir, and Temkin isotherms. These data were obtained by applying the same SPE procedure mentioned above at concentrations varying from 1 to 40 mg L⁻¹. The calculated parameters for each isotherm model are listed in Table 3, and corresponding plots are depicted in Fig. 5.

The Langmuir isotherm theory assumes that the adsorption energies are uniform and no transmigration of adsorbate in the plane of the surface occurs. This model suggests that sorption occurs at a finite number of identical homogeneous adsorbent sites, producing a monolayer on the surface of the sorbent, so once a site is occupied by adsorbate, no further sorption takes place at that site. The activities at the sites are proportional to their concentration. The general expression for this model and its linearized form are

Table 3 Langmuir and Freundlich and Temkin isotherm constants for adsorption of Co(II) ions

Langmuir isotherm			Freundlich isotherm			Temkin isotherm		
Q_m (mg g^{-1})	K_L (L mg^{-1})	R^2	n	K_F (mg g^{-1})	R^2	A_T (L mg^{-1})	b_T (kJ mol^{-1})	R^2
32.05	11.38	0.987	1.768	5.560	0.989	0.179	16.370	0.977

Conditions: pH 8, sorbent 0.05 g, concentration 1–40 mg L^{-1} , sample volume 50 mL, contact time 20 min

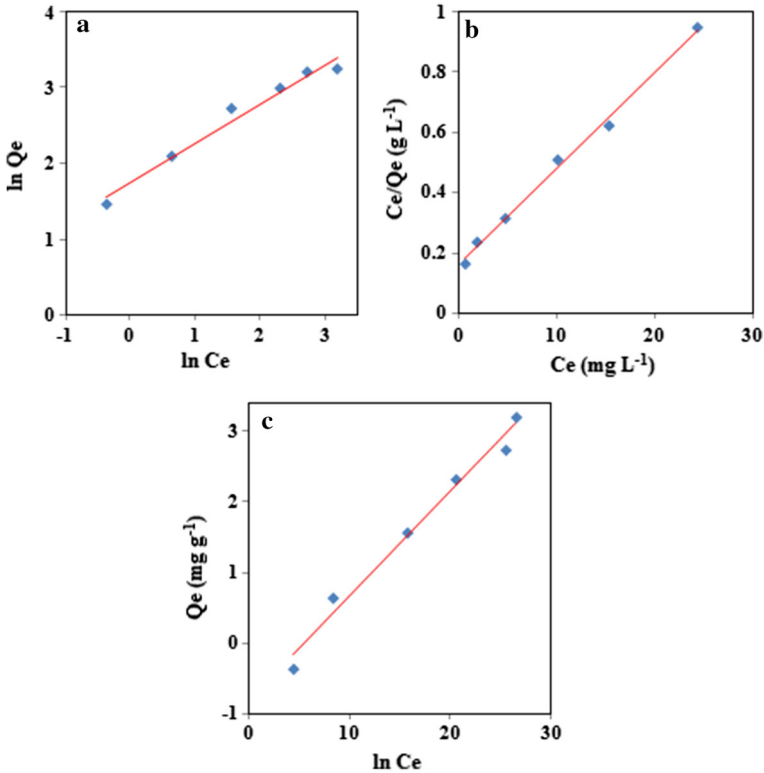


Fig. 5 **a** Freundlich, **b** Langmuir, and **c** Temkin isotherm models for Co(II) adsorption on AEPTMS-coated Fe_3O_4 nanoparticles (conditions: pH 8, dosage 0.05 g, sample volume 50 mL, concentration 1–40 mg L^{-1} , time 20 min)

$$Q_e = Q_{\max} \frac{K_L C_e}{1 + K_L C_e}, \quad (5)$$

$$\frac{Q_e}{C_e} = K_L Q_{\max} - K_L Q_e, \quad (6)$$

where Q_e is the amount adsorbed (mg g^{-1}), C_e is the equilibrium concentration of the metal ion (mg L^{-1}), Q_{\max} (mg g^{-1}) is the maximum amount of adsorbed metal

ion per unit mass of sorbent (corresponding to complete coverage of the adsorptive sites), and K_L (L mg^{-1}) is the Langmuir constant, which is related to the energy of adsorption. The parameters of this model were calculated by plotting Q_e versus $\frac{Q_e}{C_e}$.

The Freundlich model can be applied to nonideal sorption on heterogeneous surfaces and multilayer sorption. In this model, it is assumed that the sorption site energy shows an exponentially decay during the adsorption process. The Freundlich isotherm model is expressed by the following equations:

$$Q_e = K_F C_e^{1/n}, \quad (7)$$

$$\ln Q_e = \ln K_F + \frac{1}{n} \ln C_e, \quad (8)$$

where K_F is an empirical constant indicative of the sorption capacity and n is an empirical parameter indicative of the sorption intensity, which is affected by the heterogeneity of the material. Values of n between 1 and 10 indicate favorable adsorption conditions; larger values imply stronger interaction between sorbent and analyte, whereas smaller ones indicate linear adsorption leading to identical adsorption energies for all sites. Data were fit to this model by plotting $\ln Q_e$ versus $\ln C_e$ [45–47].

The Temkin isotherm model contains a factor that explicitly takes into account adsorbent–adsorbate interactions. By ignoring extremely low and high concentrations, this model assumes that the heat of adsorption of all molecules within the layer decreases linearly rather than logarithmically with coverage. As implied by the resulting equation, it is characterized by a uniform distribution of binding energies (up to some maximum). The model is formulated as

$$Q_e = \frac{RT}{b_T} \ln(A_T C_e), \quad (9)$$

$$Q_e = \frac{RT}{b_T} \ln A_T + \frac{RT}{b_T} \ln C_e, \quad (10)$$

where A_T is the Temkin isotherm equilibrium binding constant (L g^{-1}), b_T is the Temkin isotherm constant, which is related to the heat of sorption (J mol^{-1}), R is the universal gas constant ($8.31 \text{ J mol}^{-1} \text{ K}^{-1}$), and T is the temperature in kelvin [48].

The best-fit isotherm was selected based on linear regression correlation coefficient (R^2) values. As this coefficient was high (>0.995) for the Langmuir isotherm, chemisorption can be accepted as the main adsorption mechanism.

Analytical performance

The analytical performance of the current method was evaluated using the optimized experimental conditions to show its efficiency compared with other works reported in literature for determination of the same ion. These data are summarized in Table 4. The calibration curve showed linearity in the concentration range of 1–200 $\mu\text{g L}^{-1}$ with correlation coefficient of 0.9979. The limit of detection

Table 4 Comparison of published preconcentration methods for Co(II) versus the proposed method

Sorbent	PF	LOD ($\mu\text{g L}^{-1}$)	RSD (%)	LDR ($\mu\text{g L}^{-1}$)	Sorption capacity (mg g^{-1})	Extraction time (min)	Ref.
poly(AGE/IDA-co-DMAA) silica	10	0.31	3.2	–	72	240	[7]
Solid-phase microextraction- PAN	20	0.24	4.3	10–1000	–	2	[15]
Cloud-point extraction	25	1.0	3.6	250–5000	–	20	[16]
PAR/Amberlite XAD-7	200	0.10	13	0.5–5	–	45	[18]
Activated carbon	80	0.19	3.7	20–400	1.2	20	[20]
AEAPTMS/Fe ₃ O ₄	70	0.5	2.5	1–200	32.05	20	This work

PF Preconcentration factor, *LOD* limit of detection, *RSD* relative standard deviation, *LDR* linear dynamic range, *AGE/IDA* 1-(N,N-bis-carboxymethyl)amino-3-allylglycerol, *DMAA* N, N-dimethylacrylamide, *PAN* 1-(2-Pyridylazo)-2-naphthol, *PAR* 4-(2-Pyridylazo)resorcinol

(LOD) was calculated as the analyte concentration equal to three times the standard deviation of five replicates of the blank signal, yielding a value of $0.5 \mu\text{g L}^{-1}$. The precision of the method was evaluated by estimating the relative standard deviation (RSD%) for solutions containing $100 \mu\text{g L}^{-1}$ Co ions with five replicates, yielding a value of 2.5%.

Application of method

To demonstrate the applicability of the proposed method, it was applied for determination of trace amounts of Co(II) ions in a wide variety of samples. Furthermore, the accuracy of the method was checked by spiking samples with known amount of analyte. For comparison with the results of the proposed method, the analyte concentration in real samples was also determined by inductively coupled plasma atomic emission spectroscopy (ICP-AES) as a standard method before applying the preconcentration procedure. The analytical results are summarized in Table 5. Statistical analysis (paired *t* test, confidence level 95%) suggested no significance differences between the analyte concentrations as determined by the presented method versus the reference method. In view of the high selectivity provided by flame atomic absorption spectrometry, the recovery of spiked samples was satisfactory (96.6–102%), indicating the capability of the method for determination of the target ion in real samples with different matrices. It was found that the amount of Co ions was $0.04 \mu\text{g mL}^{-1}$ in malt beverage, and 3.02 and 1.85 ng g^{-1} in shrimp and radish, respectively, while Co ions were not detected in instant coffee powder, soya, or wheat bud powder.

Table 5 Analytical results for determination of Co(II) ions in real samples

Sample	Added ($\mu\text{g L}^{-1}$)	Found ($\mu\text{g L}^{-1}$)		Recovery (%)
		Proposed method	ICP-AES method	
Tap water	0	N.D.	N.D.	–
	50	49.1 \pm 0.95	50.8 \pm 0.43	98.2
Sea water	0	31.3 \pm 0.66	33.7 \pm 0.36	–
	50	80.1 \pm 0.78	82.8 \pm 0.40	98.5
Instant coffee powder	0	N.D.	N.D.	–
	50	50.4 \pm 0.74	49.0 \pm 0.35	101
Malt beverage	0	10.1 \pm 0.25	10.8 \pm 0.26	–
	50	61.2 \pm 0.60	62.8 \pm 0.47	102
Shrimp	0	30.2 \pm 0.62	28.8 \pm 0.69	–
	50	78.7 \pm 0.78	77.8 \pm 0.59	98.1
Soya	0	N.D.	N.D.	–
	50	48.3 \pm 0.40	49.1 \pm 0.47	96.6
Radish	0	18.5 \pm 0.20	17.8 \pm 0.26	–
	50	68.8 \pm 0.55	67.6 \pm 0.76	100
Wheat bud powder	0	N.D.	N.D.	–
	50	48.9 \pm 0.30	49.3 \pm 0.38	97.8

Conditions: pH 8, sorbent 0.05 g, sample volume 50 mL, eluent volume 5 mL, contact time 20 min, desorption time 10 min

N.D. Not detected

Conclusions

Amino-functionalized Fe₃O₄ nanoparticles were synthesized using a simple, green, fast, and cost-effective methodology. Successful synthesis was proved by SEM, VSM, and FTIR analyses. The adsorbent was used for preconcentration of Co(II) ions from aqueous solution using an MSPE procedure. The presented method enjoys a fast sorption desorption equilibrium due to the high specific surface area of the modified nanoparticles, the absence of internal diffusion resistance, operation in dispersion mode, and magnetic separation. In addition, functionalization of the MNPs leads to high preconcentration factor and good adsorption capacity with no foreign ion interference. Compared with similar procedures reported in literature, the proposed method exhibits wide linear range, good precision, and low detection limit. Use of the proposed method for determination of Co(II) ions in food and water samples gave acceptable results, suggesting that the procedure can be applied successfully for determination of trace amounts of this ion in complex real samples.

Acknowledgements Financial support of this study by a grant from the Research Council of the University of Tehran is gratefully acknowledged.

References

1. M. Hosseini, N. Dalali, S. Moghaddasifar, *J. Anal. Chem.* **69**, 1141 (2014)
2. N. Gault, C. Sandre, J.L. Poncy, C. Moulin, J.L. Lefaix, C. Bresson, *Toxicol. In Vitro* **24**, 92 (2010)
3. R.W. Leggett, *Sci. Total Environ.* **389**, 259 (2008)
4. J. Gál, A. Hursthouse, P. Tatner, F. Stewart, R. Welton, *Environ. Int.* **34**, 821 (2008)
5. E.J. Song, *Adv. Mater. Res.* **826**, 203 (2013)
6. S. Anttila, S. Sutinen, M. Paananen, K.E. Kreis, S.J. Sivonen, A. Grekula, T. Alapieti, *Eur. J. Respir. Dis.* **69**, 83 (1986)
7. H.A. Panahi, R.A. Kashkoieh, Mahshid Nikpour Nezhati, I.Y. G, Elham Moniri, *Korean J. Chem. Eng.* **30**, 1722 (2013)
8. H. Ciftci, *CLEAN–Soil, Air, Water* **38**, 657 (2010)
9. M. Soylak, L. Elci, M. Dogan, *Anal. Lett.* **33**, 37 (2000)
10. M.H. Baki, F. Shemirani, R. Khani, *J. Food Sci.* **78**, T797 (2013)
11. M. Soylak, B. Kaya, M. Tuzen, *J. Hazard. Mater.* **147**, 832 (2007)
12. M. Soylak, U. Divrikli, L. Elci, M. Dogan, *Talanta* **56**, 565 (2002)
13. C. Herrero Latorre, J. Alvarez Mendez, J. Barciela Garcia, S. Garcia Martin, R.M. Pena Crecente, *Anal. Chim. Acta* **749**, 16 (2012)
14. A. Uzun Karatepe, M. Soylak, L. Elci, *Anal. Lett.* **35**, 2363 (2002)
15. L. Meng, C. Chen, Y. Yang, *Anal. Lett.* **48**, 453 (2015)
16. D. Citak, M. Tuzen, *Food Chem. Toxicol.* **48**, 1399 (2010)
17. Naeemullah, M. Tuzen, T.G. Kazi, D. Citak, M. Soylak, *J. Anal. At. Spectrom.* **28**, 1441 (2013)
18. M. Ince, G. Kaya, M. Yaman, *Environ. Chem. Lett.* **8**, 283 (2010)
19. A. Duran, M. Tuzen, M. Soylak, *J. Hazard. Mater.* **169**, 466 (2009)
20. B. Feist, B. Mikula, *Food Chem.* **147**, 302 (2014)
21. F. Augusto, L.W. Hantao, N.G.S. Mogollón, S.C.G.N. Braga, *Trends Anal. Chem.* **43**, 14 (2013)
22. D. Das, U. Gupta, A.K. Das, *Trends Anal. Chem.* **38**, 163 (2012)
23. M. Šafaříková, I. Šafařík, *J. Magn. Magn. Mater.* **194**, 108 (1999)
24. M.E.S. Synaridou, V.A. Sakkas, C.D. Stalikas, T.A. Albanis, *J. Chromatogr. A* **1348**, 71 (2014)
25. Q.L. Li, L.L. Wang, X. Wang, M.L. Wang, R.S. Zhao, *J. Chromatogr. A* **1449**, 39 (2016)
26. X.S. Li, G.T. Zhu, Y.B. Luo, B.F. Yuan, Y.Q. Feng, *Trends Anal. Chem.* **45**, 233 (2013)
27. S. Mahpishanian, H. Sereshiti, *J. Chromatogr. A* **1443**, 43 (2016)
28. M. Wierucka, M. Biziuk, *Trends Anal. Chem.* **59**, 50 (2014)
29. Q. Zhou, M. Lei, J. Li, K. Zhao, Y. Liu, *J. Chromatogr. A* **1441**, 1 (2016)
30. L. Xie, R. Jiang, F. Zhu, H. Liu, G. Ouyang, *Anal. Bioanal. Chem.* **406**, 377 (2014)
31. H. Bagheri, A. Afkhami, M. Saber-Tehrani, H. Khoshafar, *Talanta* **97**, 87 (2012)
32. W. Wu, Q. He, C. Jiang, *Nanoscale Res. Lett.* **3**, 397 (2008)
33. G. Giakissikli, A.N. Anthemidis, *Anal. Chim. Acta* **789**, 1 (2013)
34. J. Abolhasani, R.H. Khanmiri, E. Ghorbani-Kalhor, A. Hassanpour, A.A. Asgharinezhad, N. Shekari, A. Fathi, *Anal. Methods* **7**, 313 (2015)
35. S.A. Jadhav, R. Bongiovanni, *Adv. Mater. Lett.* **3**, 356 (2012)
36. E.A. Smith, W. Chen, *Langmuir* **24**, 12405 (2008)
37. M.H. Mashhadizadeh, *J. Nanomed. Nanotechnol.* **3**, 3 (2012)
38. D. Dupont, W. Brullot, M. Bloemen, T. Verbiest, K. Binnemans, *ACS Appl. Mater. Interfaces* **6**, 4980 (2014)
39. J. Febrianto, A.N. Kosasih, J. Sunarso, Y.H. Ju, N. Indraswati, S. Ismadji, *J. Hazard. Mater.* **162**, 616 (2009)
40. K.G. Bhattacharyya, S. Sen Gupta, *Adv. Colloid Interface Sci.* **140**, 114 (2008)
41. Y.S. Ho, *J. Hazard. Mater.* **136**, 681 (2006)
42. M. Zarezadeh-Mehrizi, A. Badii, A. Shahbazi, *Res. Chem. Intermed.* **42**, 3537 (2016)
43. L. He, D.D. Liu, B.B. Wang, H.B. Xu, *Res. Chem. Intermed.* **41**, 3913 (2015)
44. G. Limousin, J.P. Gaudet, L. Charlet, S. Szenknect, V. Barthes, M. Krimissa, *Appl. Geochem.* **22**, 249 (2007)
45. G. Alberti, V. Amendola, M. Pesavento, R. Biesuz, *Coord. Chem. Rev.* **256**, 28 (2012)
46. S. Rangabhashiyam, E. Nakkeeran, N. Anu, N. Selvaraju, *Res. Chem. Intermed.* **41**, 8405 (2015)
47. R. Saha, K. Mukherjee, I. Saha, A. Ghosh, S.K. Ghosh, B. Saha, *Res. Chem. Intermed.* **39**, 2245 (2013)
48. K.Y. Foo, B.H. Hameed, *Chem. Eng. J.* **156**, 2 (2010)